

## **Changes in seismicity pattern due to the 2016 Kumamoto earthquake sequence**

K. Z. Nanjo<sup>1,2,3,\*</sup>, J. Izutsu<sup>4</sup>, Y. Orihara<sup>5</sup>, M. Kamogawa<sup>1</sup>, T. Nagao<sup>1,6</sup>

<sup>1</sup>Global Center for Asian and Regional Research, University of Shizuoka, 3-6-1, Takajo, Aoi-ku,

Shizuoka 420-0839, Japan

Tel: +81-54-245-5600 Fax: +81-54-245-5603

<sup>2</sup>Center for Integrated Research and Education of Natural Hazards, Shizuoka University, 836, Oya,

Suruga-ku, Shizuoka 422-8529, Japan.

<sup>3</sup>Institute of Statistical Mathematics, 10-3, Midori-cho, Tachikawa, Tokyo 190-8562, Japan.

<sup>4</sup>International Digital Earth Applied Science Research Center, Chubu University, 1200,

Matsumoto-cho, Kasugai, Aichi 487-8501, Japan.

<sup>5</sup>Tokyo Gakugei University, 4-1-1, Nukuikita-machi, Koganei, Tokyo 184-8501, Japan.

<sup>6</sup>Institute of Ocean Research and Development, Tokai University, 3-20-1, Orido, Shimizu-ku,  
Shizuoka 424-8610, Japan.

\*Correspondence to: [nanjo@u-shizuoka-ken.ac.jp](mailto:nanjo@u-shizuoka-ken.ac.jp)

## **Highlights**

- Seismicity analysis implies stress disturbance due to the 2016 Kumamoto earthquakes
- Stress field revealed aseismic pre- and after- slow slip around the causative fault
- Pre-slip induced local stress reduction near the eventual mainshock hypocenter

## **Abstract**

Crustal deformation due to the 2016 earthquake sequence in Kumamoto, Japan, that culminated in a preceding earthquake of magnitude  $M6.5$  and a subsequence  $M7.3$  earthquake 28 hours later, caused stress perturbation on and around the causative Futagawa-Hinagu fault zone. Monitoring changes in seismicity pattern along this zone plays a role in understanding the process before and after major earthquakes. For this purpose, we used stress-dependent laws in statistical seismology: the Gutenberg-Richter frequency-size law and the Omori-Utsu aftershock-decay law. Results obtained by using these laws show a zone of high stress near the eventual epicenters of the  $M6.5$  and  $M7.3$  earthquakes before the start of the Kumamoto sequence, and after it, a decreasing trend in stress along the Futagawa-Hinagu fault zone. Our detailed analysis suggests an aseismic pre- and after-slip along the causative fault zone, which is consistent with other geophysical observations. The pre-slip locally reduced stress just prior to the  $M7.3$  earthquake near its epicenter. Recently, a system was proposed by Gulia and Wiemer (2019) that utilizes the Gutenberg-Richter frequency-size law to judge, immediately after a large earthquake, whether it was the mainshock or a foreshock to a future event. A comparison of results suggests that further research is needed to improve this system to take into consideration the spatial variation of frequency-size distribution that allows the exploration of the possibility of a local pre-slip of a future nearby earthquake.

**Keywords**

Seismicity, Earthquake interaction, Computational seismology, Continental tectonics, Stresses,  
Probabilistic forecasting

## 1. Introduction

The 2016 Kumamoto earthquake sequence (Fig. 1) that brought about serious damage to Kumamoto, in central Kyushu, Japan (Hashimoto et al., 2017), began with an earthquake of magnitude ( $M$ ) 6.5 on April 14, 2016, at 21:26, on the northern section of the Hinagu fault zone (FZ), which was followed by numerous events, including a  $M6.4$  earthquake on April 15, at 00:03. These  $M6.5$ -class earthquakes, which were considered as foreshocks, involved a predominantly right-lateral strike slip. Eventually, on April 16, at 01:25, a  $M7.3$  mainshock occurred on the Futagawa FZ that conjugated with the northern section of the Hinagu FZ, revealing a similar mechanism of fault motion as the  $M6.5$ -class foreshocks. The  $M7.3$  mainshock started at the westernmost part of the Futagawa FZ, and its rupture propagated toward the east and terminated around Mt. Aso (Yagi et al., 2016). Over the first three years since the  $M7.3$  mainshock (Fig. 1b), more than 27,000 aftershocks with  $M \geq 1$  occurred, including more than 100 events with  $M \geq 4$ . The Earthquake Research Committee (ERC) concluded that the Futagawa FZ and the northern section of the Hinagu FZ have been activating (ERC, 2016a). The probability of the occurrence of an approximately  $M7.0$  earthquake on the Futagawa FZ had been estimated to be 0-0.9% within 30 years, which was rather high among the probability at active faults in Japan (ERC, 2016a). For the northern section of the Hinagu FZ, it was possible that an approximately  $M6.8$  earthquake might occur, although the probability of the earthquake occurrence within 30 years was uncertain (ERC, 2016a).

The broader context of the Kumamoto earthquakes is that the Futagawa-Hinagu FZ is encompassed by the Beppu–Shimabara graben, a geological formation that runs across the middle of Kyushu, from Beppu Bay in the east to the Shimabara Peninsula in the west (Inset of Fig. 1). This is understood as being the result of crustal deformation caused by the rifting and spreading of the Okinawa Trough, which is viewed as a continuation of the Beppu–Shimabara graben (Tada 1985). Under such tectonic conditions, the Kumamoto earthquakes occurred in a seismically active region.

Monitoring crustal deformation and seismicity along the causative faults plays a role in understanding the process before and after major earthquakes. Numerical simulation and rock mechanics experiments suggest the occurrence of pre- and post-seismic slip transients. Some studies implied long-term precursory slip acceleration while other studies indicated a nucleation process that initially involves stable and slow rupture growth (Hori and Miyazaki, 2010; Yoshida and Kato, 2003; Dieterich, 1979; Lapusta et al., 2000). However, it is generally accepted that a precursory slip before a large earthquake is not always observed. This may be because the phenomenon did not always emerge in nature and/or due to difficulty in observing a small slip. On the other hand, a post-seismic slip was observed for many earthquakes.

Recognizing earthquakes as foreshocks in real time would provide a valuable forecasting capability. However, decades of work have failed to establish a robust feature of individual foreshocks that distinguishes them from mainshocks or their aftershocks (Dascher-Cousineau et al.,

2020). Foreshocks may be distinctive due to some precursory loading process or influence from the locked zone of the subsequent mainshock, neither of which will exist in the aftershock sequence (Brody and Lay, 2014). A fundamental question regarding the Kumamoto sequence is whether or not any indication of an impending large earthquake had appeared before the  $M7.3$  mainshock. The Japan Meteorological Agency (JMA) held a press conference after the  $M6.5$  earthquake to warn of the possibility of large aftershocks with further damage. However, the JMA did not consider the occurrence of large earthquakes, according to the ERC (1998) protocol (see also ERC, 2016b), so no information was made public on the increased probability of  $M7$  or larger earthquakes.

In a recent study, Gulia and Wiemer (2019) proposed a Foreshock Traffic-Light System (FTLS) that relies on abrupt changes in  $b$ -values of the Gutenberg-Richter (GR) frequency-magnitude law (Gutenberg and Richter, 1944), relative to background values. The approach utilizes high-resolution earthquake catalogs to monitor localized regions around the largest earthquakes and to distinguish foreshock sequences (reduced  $b$ -values) from aftershock sequences (increased  $b$ -values) (Gulia et al., 2020; Dascher-Cousineau et al., 2020). Evidence supporting the FTLS hypothesis emerged from investigating a time series of two sequences: the Norcia, Italy, sequence and the Kumamoto sequence. Their results of the Kumamoto case showed that  $b$ -values in the time interval between the  $M6.5$  and  $M7.3$  events first dropped from the background level and then increased over time, and that the  $b$ -values at the intermediate and ending times were below the

background level, triggering a red traffic light and suggesting that seismicity in between was not considered as an aftershock sequence, rather as a foreshock one. Once the  $M7.3$  mainshock occurred,  $b$ -values of the subsequent events increased strongly by 20-40%, triggering a green traffic light, suggesting that these events were aftershocks.

Slow deformation caused by a post-seismic slip of the causative Futagawa-Hinagu FZ and flow in the Earth's interior has been observed in the aftermath of the Kumamoto earthquakes, detected by data from the GEONET: GNSS Earth Observation Network System. This deformation was modeled by joint after-slip and viscoelastic relaxation at depths driven by the Kumamoto coseismic ruptures (Moore et al., 2017; Pollitz et al., 2017). Viscoelastic modeling strongly favors a very weak lower crust associated with the Beppu-Shimabara graben and the locus of central Kyushu volcanism (Pollitz et al., 2017). The coseismic ruptures and post-seismic deformation, which caused stress perturbation along the Futagawa-Hinagu FZ, play a crucial role in understanding the seismicity pattern and distribution of seismic hazards (Moore et al., 2017).

In this study, we focused on the fact that the Kumamoto earthquakes occurred within a seismically active region, with data of good enough quality and sufficient abundance, collected by the JMA. To explore the process before and after the Kumamoto mainshock, we used the  $b$ -value of the GR law and the  $p$ -value of the Omori-Utsu (OU) aftershock-decay law (Utsu, 1961), both explained in the next section. The  $b$ -value is inversely proportional to differential stress, and the

$p$ -value can be used to infer stressing history. Characteristics of seismicity before, during, and after the Kumamoto earthquakes were investigated. The main conclusion is that local and time-dependent variation in  $b$ - and  $p$ -values are linked with crustal deformation due to coseismic and aseismic slips along the Futagawa-Hinagu FZ and viscoelastic relaxation of the lower crust and upper mantle associated with the Beppu-Shimabara graben. Moreover, we discuss whether or not the Kumamoto sequence is a good example to demonstrate the FTLS, based on our results (Nanjo et al., 2016, 2019; Nanjo and Yoshida, 2017).

## 2. Data and Method

The GR law (Gutenberg and Richter, 1944) is given as

$$\log_{10}N = A - bM, \tag{1}$$

where  $N$  is the cumulative number of earthquakes with a magnitude larger than or equal to  $M$ ,  $A$  characterizes seismic activity or earthquake productivity of a region, and the constant  $b$  is used to describe the relative occurrence of large and small events (i.e., a high  $b$ -value indicates a larger proportion of small earthquakes, and *vice versa*). Spatiotemporal changes in  $b$  are known to reflect a state of stress in the Earth's crust (Narteau et al., 2009; Schorlemmer et al., 2005; Scholz, 2015) and

to be influenced by asperities and frictional properties (Schorlemmer et al., 2004; Schorlemmer & Wiemer, 2005; Tormann et al., 2013) and by interface locking along subduction zones (e.g. Ghosh et al., 2008, Nanjo & Yoshida, 2018, Sobiesiak et al., 2007, Tormann et al., 2015). The results of laboratory experiments indicate a systematic decrease in the  $b$ -value approaching the time of the entire fracture (Lei, 2003; Scholz, 1968). To estimate  $b$ -values consistently over space and time, we employed the EMR (entire-magnitude range) technique (Woessner & Wiemer, 2005), which also simultaneously calculates the completeness magnitude  $M_c$ , above which all events can be detected by a seismic network. EMR applies the maximum-likelihood method to compute the  $b$ -value to events with a magnitude above  $M_c$ . Uncertainties in  $b$  were computed by bootstrapping (Schorlemmer et al., 2003). If  $\log P_b$ , the logarithm of the probability that the  $b$ -values are not different, is equal to or smaller than -1.3 ( $\log P_b \leq -1.3$ ), then the change in  $b$  is significant (Utsu, 1999; Schorlemmer et al. 2004).

The OU law (Utsu, 1961) is given as

$$\lambda = k(c + t)^{-p}, \tag{2}$$

where  $t$  is the time since the occurrence of a mainshock,  $\lambda$  is the number of aftershocks per unit time at  $t$  with  $M$  greater than or equal to a cutoff magnitude, and  $c$ ,  $k$ , and  $p$  are constants.  $p = 1$  is

generally a good approximation (Omori, 1894). Similar to the GR case, we used the maximum-likelihood fit to determine the parameters for this law. Uncertainties in  $p$  were computed by bootstrapping. The rate- and state-dependent friction law (Dieterich, 1994) assumes  $p = 1$  as a standard form. Variability in  $p$  is possible:  $p > 1$  and  $p < 1$  for special cases with rapidly and slowly decreasing stress, respectively.

Our dataset was the earthquake catalog maintained by the JMA. We used about  $10^6$  earthquakes having  $M \geq 0$  during the period from January 1, 2000 to March 23, 2019 with depths shallower than 25 km within the study region (Fig. 1). The catalog was pre-cut into three sub-catalogs to consider different time periods to find time-dependent signals that are consistent with stress increase and release: about 16 years before the  $M6.5$  foreshocks, 28 hours after the  $M6.5$  event, and about 3 years after the  $M7.3$  mainshock.

In addition to the Kumamoto earthquakes, two  $M5$ -class earthquakes occurred in the study region: one was the  $M5.0$  event in 2000 near the epicenter of the  $M7.3$  mainshock, and the other was the  $M5.1$  event on January 3, 2019, 20 km northwest of the Futagawa FZ. The ERC (2019) announced that the latter earthquake was unrelated to the Kumamoto earthquakes. Both events are thus not considered as the Kumamoto earthquakes.

### 3. Results

### 3.1. Pre- $M6.5$ -quake sequence

We first considered the sequence before the start of the Kumamoto sequence. A map view of  $b$ -values before the  $M6.5$  foreshock reveals a zone of low  $b$ -values near the eventual epicenters of the  $M7.3$  mainshock and two  $M6.5$ -class foreshocks (Fig. 2). The characteristic dimension of unusually low  $b$ -values in an approximately  $0.3^\circ \times 0.3^\circ$  area in Fig. 2 is  $\approx 30$  km. The  $M5$  earthquake on June 8, 2000, occurred near the mainshock epicenter, so we analyzed a  $b$ -value time series in the inset of Fig. 2 (also see Fig. A4 of Nanjo and Yoshida, 2017) and created sequential maps of  $b$ -values (Fig. A2 of Nanjo et al., 2016) to show that a zone of low  $b$ -values is insensitive to the 2000  $M5$  earthquake and that this earthquake is not the main cause of the low spatially mapped  $b$ -values in Fig. 2.

### 3.2. Post- $M6.5$ -quake sequence

We next considered the sequence between the  $M6.5$  and  $M7.3$  earthquakes. A cumulative curve of  $M \geq 3$  events (Fig. 3b) indicates two kinks at 0.98 and 0.67 days before the  $M7.3$  mainshock, suggesting seismicity quiescence, that is, transitions to lower occurrence rates happened twice. To create this figure, we truncated the catalog at  $M = 3$  in advance to discard all data that may have been inhomogeneous, based on  $M_c$  in Fig. 3a. The same plotting procedure as Fig. 3b was employed for samples from the northern area (higher than  $32.72^\circ\text{N}$ ) and the southern area (lower than  $32.72^\circ\text{N}$ ),

again showing two kinks at the same times, 0.98 and 0.67 days, in both samples (Fig. 2 of Nanjo and Yoshida, 2017). The timing of the kinks did not correspond to the occurrence of the  $M6.4$  foreshock (star at 1.05 days preceding the  $M7.3$  mainshock), indicating that this event did not affect foreshock activity as a whole. Further analysis (Figs. 2, A1, and A2 of Nanjo and Yoshida, 2017) showed that the transition to a lower occurrence rate at 0.98 days relative to the  $M7.3$  mainshock was significant, but the transition at 0.67 days might not have been. Seismicity quiescence during the period between the  $M6.5$  and  $M7.3$  events was also found by Zhuang et al. (2017).

Assuming the  $M6.5$  foreshock to be a mainshock, Fig. 4b shows that the OU law in Eq. (2) with  $p = 1.49 \pm 0.29$  was correlated with seismic activity of  $M \geq 3$  for the entire area during the period between the  $M6.5$  and  $M7.3$  earthquakes (black point on right end in Fig. 4a). For a short time period (0-0.18 days, equivalent to 1.16-0.98 days preceding the  $M7.3$  mainshock),  $p = 0.46 \pm 0.14$  (black point on left end of Fig. 4a). The difference in  $p$  between these long and short periods is statistically significant, showing faster decay of seismic activity as period increased. The influence of period on  $p$  is shown in Fig. 4a (black points). We conducted the same analysis for events in the northern and southern areas (cyan and pink points, respectively). The difference in  $p$  between these areas is significant for periods longer than 0.5 days. It can be said that the rapid decrease in the number of  $M \geq 3$  events in the northern area was responsible for the rapid decay in activity observed over the entire area.

A comparison of  $b$  between two periods (1.16-0.98 and 0.98-0 days) prior to the  $M7.3$  mainshock (Figs. 5a,b) shows that the  $b$ -values increased over time. This increase was significant for the northern area with a large increase in  $b$  ( $\Delta b_1 \geq 0.3$ , blue in Fig. 5c) and low values ( $\log P_b \leq -1.3$ , green in Fig. 5d), where  $\Delta b_1 (= b_{0.98-0} - b_{1.16-0.98})$  is the subtraction of the  $b$ -value used in Fig. 5a for the period 1.16-0.98 days prior to the  $M7.3$  mainshock ( $b_{1.16-0.98}$ ) from that used in Fig. 5b for the period 0.98-0 days prior to it ( $b_{0.98-0}$ ). Results demonstrate that the changes in  $b$  were physically meaningful and not caused by artifacts (also see Nanjo and Yoshida (2017), who conducted analyses to support this observation).

Earthquakes had occurred near the hypocenter of the  $M7.3$  mainshock in addition to the majority of seismicity around the northern section of the Hinagu FZ. Fig. 6 shows a 5-km wide cross section nearly perpendicular to the strike of the Futagawa FZ, on which the rupture of the  $M7.3$  mainshock occurred. Note that several events are recognized close to the hypocenter of the  $M7.3$  mainshock (bold squares in the upper-left-corner inset of Fig. 6). In the magnitude–time diagram (lower-right-corner inset of Fig. 6), where these events are designated again by bold squares, they occurred during the period 0.98-0 days preceding the  $M7.3$  mainshock. Our result that earthquakes occurred near the eventual  $M7.3$  mainshock later on is supported by an independent observation (Kato et al., 2016).

### 3.3. Post-M7.3-quake sequence

A map view (Fig. 7) of  $b$ -values based on seismicity over the period since January 1, 2017 reveals an area of low  $b$ -values ( $b \sim 0.7$ , light blue), which lies further to the southwest of the  $M6.5$ -class foreshocks (red stars). To show this map, we did not consider the period from immediately after the mainshock to the end of 2016 to remove the effect of the main aftershock sequence that reveals strong temporal variability in  $b$  (Nanjo et al., 2019). The characteristic dimension of this low- $b$ -value area in approximately  $0.1$ - $0.2^\circ$  is  $10$ - $20$  km. We compared this map with the distribution of  $M \geq 5$  earthquakes that occurred during the period from the start of the Kumamoto sequence to the end of 2016 (stars, squares, and circles). This low- $b$ -value area is located near the southern end of  $M \geq 5$  earthquakes.

A comparison of the maps in Figs. 2 and 7 shows an increase in  $b$ -values in most areas along the Futagawa-Hinagu FZ, expected by a release of stress, presumably due to the coseismic ruptures and aftershocks. However, there is an exceptional area showing a decrease in  $b$ , which coincides with the area of low  $b$ -values (Fig. 7). This decrease in  $b$ -values is significant (upper-left-corner inset of Fig. 7), because  $\log P_b = -2.75$  for the difference in  $b$ ,  $\Delta b_2 = b_{\text{post}} - b_{\text{pre}}$ , between the  $b$ -value before the start of the Kumamoto sequence ( $b_{\text{pre}}$ ) and the  $b$ -value since 2017 ( $b_{\text{post}}$ ) in the red rectangular region of Fig 7. For nine regions along the Futagawa-Hinagu FZ (Fig. 8a),  $\Delta b_2 \geq 0$  was observed for all regions, except for Region 6, which is the same as the red

rectangular region in Fig. 7. This is interpreted as an indication of overall stress release along this FZ with a local stress-increasing region. The difference in  $b$  ( $\Delta b_2$ ) is significant, except for Regions 7 and 9, which are located farther south so that the influence of coseismic ruptures on stress perturbation in the regions is interpreted to be less pronounced.

For Regions 1-6,  $p$ -values are 1-1.4, while for Regions 7-9,  $p$ -values are below a typical value ( $p < 1$ ) if unreliable estimates are not taken into consideration (Fig. 8b). The difference in  $p$  between the northern and southern regions of the Hinagu FZ is significant while considering uncertainties in  $p$ . The feature in Fig. 8 is similar to the analysis shown in Fig. S2 of Nanjo et al. (2019). The decay of seismic activity was faster in the northern regions than in the southern ones. A summary of results of  $b$ - and  $p$ -value analysis are provided in Fig. 8c.

## 4. Discussion

### 4.1. Pre- $M6.5$ -quake sequence and aseismic faulting

Prior to the start of the 2016 Kumamoto earthquakes, the location of stress concentration (low  $b$ -value) was regarded as a candidate of the initiation of dynamic ruptures for the  $M6.5$ -class foreshocks and the  $M7.3$  mainshock (Fig. 2). This was consistent with other observations in previous studies that correlated patches of low  $b$ -value, with the large earthquakes in California, Tohoku-oki, Sumatra, and others (Schorlemmer and Wiemer, 2005; Nanjo et al., 2012; Tormann et al., 2013,

2015; Nanjo, 2020). The combined evidence in those studies indicates that  $b$ -values can be used to predict a highly stressed area, into which nucleation points of eventual ruptures are included.

Although some cases showed success in detecting a decrease in  $b$ -value prior to large earthquakes at a decade-scale lead time (Nanjo et al., 2012; Tormann et al., 2015; Nanjo, 2020), the precursory duration to the  $M7.3$  mainshock is unknown from the application of the  $b$ -value method to data over the past 16 years. The timing of the earthquake remains uncertain from a low  $b$ -values time series (lower-right-corner inset of Fig. 2) and sequential  $b$ -value maps prior to the start of the Kumamoto earthquakes (Nanjo et al., 2016). This is consistent with another observation of active faults in which the heterogeneous pattern of  $b$ -values at Parkfield was, to a high degree, stationary for the past 35 years and the 2004  $M6$  earthquake eventually occurred at a zone of low  $b$ -values (Schorlemmer and Wiemer, 2005). A decrease in  $b$  tracking stress buildup, as expected from a laboratory experiment (Scholz, 1968; Lei, 2003), might not be observable for the decade-scale observation of active faults, because it is too short to observe such a decrease in  $b$  for the Kumamoto and Parkfield cases. Instead, the stationary nature of  $b$ -values, as observed in Fig. 2, is reasonable. The mechanism of stress buildup within the fault zones is uncertain, but one hypothesis is that a steady slip of the deeper continuation of faults that does not produce earthquakes, but still involves motions across the fault, forces the upper crust around the faults to deform, and thus concentrate stress. This is still difficult to measure directly.

#### 4.2. Post-*M*6.5-quake sequence and pre-slip

Our analysis based on seismicity during the period from the *M*6.5 foreshock to the *M*7.3 mainshock indicates an increase in the *p*- and *b*-values in the northern area (Figs. 4 and 5). This finding suggests that stress around the Futagawa FZ had begun to decrease preceding the *M*7.3 mainshock, if we considered that a high *p*-value does not indicate an increase in stress (Dieterich, 1994) and that a high *b*-value indicates low stress (Scholz, 1968, 2015).

The reduction in normal stress at the Futagawa FZ, i.e., a decrease in compressive stress on the fault, was suggested by an independent observation from the National Research Institute for Earth Science and Disaster Resilience (2016). A temporal change in the stress field by performing a stress inversion analysis using focal mechanisms of earthquakes in and around the Kumamoto earthquakes was examined. The minimum compressive stress ( $\sigma_3$ ) axis lay roughly in a north-south axis before the *M*6.5 foreshock. From  $\sigma_3$ -axes before and after the *M*6.5 foreshock, the axis rotated counterclockwise and became nearly perpendicular to the strike of the Futagawa FZ, which indicates a reduction in normal force acting on the fault plane.

We also found that earthquakes had occurred near the hypocenter of the *M*7.3 mainshock (Fig. 6). One possible explanation may be that they were produced by a nucleation process, as suggested by Onaka (1993), of the *M*7.3 mainshock. Our finding of the occurrence of earthquakes

close to the  $M7.3$  hypocenter (Fig. 7), combined with a reduction of normal pressure on the Futagawa FZ (National Research Institute for Earth Science and Disaster Resilience, 2016), indicates the growth of a quasi-static pre-slip before the  $M7.3$  mainshock. This pre-slip might have relaxed stress around the hypocenter of the  $M7.3$  mainshock. This stress relaxation provided feedback, causing a significantly larger  $p$ -value than  $p = 1$  (Fig. 4) and a significant increase in the  $b$ -value (Fig. 5) in the northern area, including a part of the Futagawa FZ that hosted the forthcoming  $M7.3$  mainshock.

#### *4.3. Post- $M7.3$ -quake sequence and after-slip*

Our analysis based on seismicity after January 1, 2017 pinpointed an area of low  $b$ -values along the Futagawa-Hinagu FZ (Fig. 7). This is the only area where the  $b$ -value had significantly decreased, compared to the  $b$ -value of the pre-Kumamoto seismicity (Figs. 2 and 7). Furthermore, the low- $b$ -value area for seismicity in and after 2017 is located at the southernmost area of the activated northern section of the Hinagu FZ, beyond which no  $M5$ -class earthquakes occurred (Fig. 7).

Pollitz et al. (2017) assumed after-slip planes representing the Futagawa FZ and the northern section of the Hinagu FZ (Fig. 7). The south end of after-slip planes representing the latter is near the south end of  $M5$ -class aftershocks. Pollitz et al. (2017) found that a shallow after-slip

dominated the post-seismic relaxation in the near field, while viscoelastic relaxation of the lower crust and mantle dominated at a greater distance. The Futagawa FZ and the northern section of the Hinagu FZ are included in the after-slip-dominant regime causing a rapid decrease in stress, and the southern section of the Hinagu FZ is in the viscoelastic-flow-dominant regime, slowly decreasing stress.

Although the overall trend in stress decreased along the Futagawa-Hinagu FZ, the after-slip on the northern section of the Hinagu FZ, in contrast to the lack of an after-slip on the southern section of the same FZ, might not lead to a decrease in local stress at the boundary between the northern and southern sections, but rather to a constant or even an increase in local stress there. If we consider a model for seismicity rate resulting from stressing history (Figure 8 of Dieterich, 1994), this explains our result (Fig. 8): High  $p$ -values ( $p > 1$ ) in the Futagawa FZ and the northern section of the Hinagu FZ are due to rapidly decreasing stress, low  $p$ -values ( $p < 1$ ) in the southern section of the Hinagu FZ are due to slowly decreasing stress, and  $p \sim 1$  near the boundary between the northern and southern sections is due to constant or increasing stress. This is supported by our prior observation (Fig. S3 of Nanjo et al., 2019) that relatively time-independent  $b$ -values based on the main aftershock sequence (until the end of 2016) are shown for a region around the south end of the northern section of the Hinagu FZ, although other along-fault regions exhibited decreasing stress (increasing  $b$ -values).

We further conducted a detailed analysis of  $b$ -values by dividing seismicity from January 1, 2017 to March 11, 2019 into two sub-data sets: one before January 1, 2018 (Nanjo et al., 2019) and one after it (lower-right-corner inset of Fig. 7). Low  $b$ -values (blue to light blue) broadly distributed before January 1, 2018 (Nanjo et al., 2019) became narrowly distributed after this date (lower-right-corner inset of Fig. 7). The low  $b$ -values are interpreted as an indication of a highly stressed area in the south end of the same section, implying that an after-slip on the causative faults continued at least over a three-year period.

Fig. 8c summarizes all of the post-Kumamoto observations and our stress model along the Futagawa-Higanu FZ. Overall consistency between our seismicity analysis and the results of geodesy indicates that changes in seismicity pattern in and around the Futagawa-Hinagu FZ reflect post-seismic deformation following the Kumamoto earthquakes.

Calculation of Coulomb stress imparted by the  $M7.3$  mainshock and  $M6.5$  foreshock to the surrounding major FZs does not provide information to explain aftershocks on and very near the Futagawa FZ and the northern section of the Hinagu FZ that ruptured during these earthquakes (Stein and Toda, 2016), so we think that it cannot be used to interpret the observed changes in  $b$  and  $p$  based on such aftershocks.

#### *4.4. FTLS applicable to the Kumamoto earthquakes?*

A general trend of the time-dependent increase in  $b$  in the interval between the  $M6.5$  and  $M7.3$  events, which had been shown by Gulia and Wiemer (2019), was also found in Fig. 5. However, if we considered the southern and northern areas separately, our analysis of  $b$ -values implied a yellow FTLS status for the former area and a green FTLS status for the latter area. For the northern area, which includes a part of the Futagawa FZ on which the impending  $M7.3$  mainshock occurred,  $b$ -values showed an increase over time, to values exceeding 1.0 (Fig. 5a,b), significantly larger than the background levels ( $b = 0.81\sim 0.83 \pm 0.05\sim 0.07$ ) found by Gulia and Wiemer (2019) and those ( $b = 0.6\sim 0.8$ ) in the area of the  $M6.5$  and  $M7.3$  epicenters (Fig. 2). On the other hand, for the southern area, which includes a part of the northern section of the Hinagu FZ on which the  $M6.5$  foreshock had already occurred,  $b$ -values were similar to or below the background level. Our results for the northern area (indicative of green FTLS status) suggested a scenario of a reduction in stress induced by growth of aseismic pre-slip on the Futagawa FZ, leading to a subsequently much larger chance of a stronger  $M7.3$  event, as discussed in section 4.2 (also see Nanjo and Yoshida, 2017). The results by Gulia and Wiemer (2019) (indicative of red FTLS status) suggested an alternative scenario in which stress on the Futagawa FZ increased, leading to a subsequently much larger chance of a stronger  $M7.3$  event. The discrepancy between our study and the Gulia and Wiemer (2019) study is that the former study investigated spatial variation of  $b$ -values, allowing us to find clues of a pre-slip on the nearby Futagawa FZ, which were not found by the latter study. The Kumamoto case might

not be a good application of the FTLS.

The picture changes markedly after the  $M7.3$  mainshock, with the  $b$ -values in the Kumamoto source area (Regions 1-5) increased significantly (Fig. 8a). This is consistent with the findings by Gulia and Wiemer (2019), who suggested that the chance of a subsequent large event was substantially small, although the Kumamoto aftershock sequence included many small events. No subsequent large event has occurred so far.

The FTLS system is quite new, and some cases, except for the Kumamoto one, would provide support for it. We agree with Gulia et al. (2020) that it is too early to use the current-version of the FTLS routinely for making decisions about civil protection and public communications. More extensive tests of sensitivity and robustness are needed, as pointed out by those authors. Based on our studies, it would be very worthwhile to improve the FTLS in ways that would allow spatial variability of  $b$ -values to be taken into consideration, and if an indication of a pre-slip appeared, this would trigger a red traffic light.

## 5. Conclusion

Using the  $b$ -value of the GR frequency-magnitude law in Eq. (1) and the  $p$ -value of the OU aftershock-decay law in Eq. (2), we showed that a zone of low  $b$ -values (indicative of high stress) lay near the eventual epicenters of the  $M6.5$  and  $M7.3$  earthquakes before the start of the

Kumamoto sequence (Fig. 2), and that after it, the overall trend in stress decreased along the Futagawa-Hinagu FZ (Figs. 2, 7, and 8). Our detailed analysis suggests an aseismic pre- and after-slip along the causative FZ (Figs. 3-8), consistent with results after performing a stress inversion analysis (National Research Institute for Earth Science and Disaster Resilience, 2016) and by using data from GEONET to detect crustal deformation (Pollitz et al., 2017). Stress reduction just prior to the  $M7.3$  mainshock near its epicenter (Figs. 4-6) was suggested to be locally induced by a pre-slip. We noted that our observed  $b$ -values were indicative of a green FTLS status before the  $M7.3$  event, in contrast to a red FRLS status shown by Gulia and Wiemer (2019), who did not study spatial variability of  $b$ -values that helped to detect an aseismic pre-slip that occurred locally on the Futagawa FZ. In our view, taking this  $b$ -value variability into account, together with using other seismological and geological information such as  $p$ -values and the spatial configuration of active faults, is important to improve the FTLS. It would also be of interest for future work to improve FTLS, taking into account the triggering of a red traffic light when signals are detected, suggesting an ongoing pre-slip.

#### **CRedit authorship contribution statement**

**K. Z. Nanjo:** Conceptualization, Funding acquisition, Formal analysis, Methodology, Software, Writing -original draft, Writing -review & editing. **J. Izutsu:** Conceptualization, Funding

acquisition, Writing -review & editing. **Y. Orihara:** Conceptualization, Writing -review & editing.

**M. Kamogawa:** Conceptualization, Writing -review & editing. **T. Nagao:** Conceptualization, Writing -review & editing.

### **Declaration of competing interests**

The authors declare that they have no known competing financial interests or personal relationships that could have appeared to influence the work reported in this paper.

### **Acknowledgements**

The authors thank the JMA for the earthquake catalog. This study was partially supported by the Ministry of Education, Culture, Sports, Science and Technology (MEXT) of Japan, under its The Second Earthquake and Volcano Hazards Observation and Research Program (Earthquake and Volcano Hazard Reduction Research), JSPS KAKENHI Grant Number JP 20K05050, the Collaboration Research Program of IDEAS, Chubu University IDEAS201812, Tokio Marine Kagami Memorial Foundation, and the Chubu Electric Power's research based on selected proposals.

The seismicity analysis software package ZMAP (Wiemer, 2001), used for Figs. 2 and 4, 5, 7, and 8, was obtained from <http://www.seismo.ethz.ch/en/research-and-teaching/products-software/software/ZMAP>. The

Generic Mapping Tools (Wessel et al., 2013), used for Figs. 1, 2, and 5-8, are an open-source collection (<https://www.generic-mapping-tools.org>).

### **Data availability**

The JMA earthquake catalog used in this study was obtained from <http://www.data.jma.go.jp/svd/eqev/data/bulletin/index.html>. We obtained the after-slip planes shown in Fig. 7 from those shown in Fig. 1 of Pollitz et al. (2017). Surface ruptures shown in Fig. 7 were obtained from Additional files of Shirahama et al. (2016).

### **References**

- Brodsky, E.E., Lay, T., 2014. Recognizing foreshocks from the 1 April 2014 Chile earthquake. *Science* 344 (6185), 700-702. <https://doi.org/10.1126/science.1255202>.
- Dascher-Cousineau, K., Lay, T., Brodsky, E.E., 2020. Two foreshock sequences post Gulia and Wiemer (2019). *Seismol. Res. Lett.* 91 (5), 2843-2850. <https://doi.org/10.1785/0220200082>.
- Dieterich, J.H., 1979. Modeling of rock friction: 1. Experimental results and constitutive equations. *J. Geophys. Res.* 84 (B5), 2161-2168. <https://doi.org/10.1029/JB084iB05p02161>.
- Dieterich, J., 1994. A constitutive law for rate of earthquake production and its application to earthquake clustering. *J. Geophys. Res.* 99 (B2), 2601-2618.

<https://doi.org/10.1029/93JB02581>.

Earthquake Research Committee, 1998. Probabilistic evaluation method of aftershocks.

<http://www.jishin.go.jp/main/yoshin2/yoshin2.htm> (In Japanese), Accessed April 2, 2021.

Earthquake Research Committee, 2016a. Evaluation of the 2016 Kumamoto earthquakes.

<https://www.jishin.go.jp/main/index-e.html> (In Japanese), Accessed April 2, 2021.

Earthquake Research Committee, 2016b. Information on perspective of seismicity after large

earthquakes. [http://www.jishin.go.jp/reports/research\\_report/yosoku\\_info/](http://www.jishin.go.jp/reports/research_report/yosoku_info/). Accessed April 2,

2021.

Earthquake Research Committee, 2019. Evaluation of earthquake in the Kumamoto region,

Kumamoto prefecture on January 3, 2019. <https://www.jishin.go.jp/main/index-e.html>,

Accessed April 2, 2021.

Ghosh, A., Newman, A.V., Thomas, A.M., Farmer, G.T., 2008. Interface locking along the

subduction megathrust from *b*-value mapping near Nicoya Peninsula, Costa Rica. *Geophys. Res.*

*Lett.* 35, L01301. <https://doi.org/10.1029/2007GL031617>.

Gulia, L., Wiemer, S., 2019. Real-time discrimination of earthquake foreshocks and aftershocks.

*Nature* 574, 193-199. <https://doi.org/10.1038/s41586-019-1606-4>.

Gulia, L., Wiemer, S., Vannucci, G., 2020. Pseudoprospective evaluation of the foreshock traffic-

light system in Ridgecrest and implications for aftershock hazard assessment. *Seismol. Res.*

Lett. 91 (5), 2828-2842. <https://doi.org/10.1785/0220190307>.

Gutenberg, B., Richter, C.F., 1944. Frequency of earthquakes in California. *Bull. Seismol. Soc. Amer.* 34 (4), 185-188.

Hashimoto, M., Savage, M., Nishimura, T., Horikawa H., Tsutsumi, H., 2017. Special issue “2016 Kumamoto earthquake sequence and its impact on earthquake science and hazard assessment”. *Earth Planets Space* 69, 98. <https://doi.org/10.1186/s40623-017-0682-7>.

Himematsu, Y., Furuya, M., 2016. Fault source model for the 2016 Kumamoto earthquake sequence based on ALOS-2/PALSAR-2 pixel-offset data: Evidence for dynamic slip partitioning. *Earth Planets Space* 68 (1), 169. <https://doi.org/10.1186/s40623-016-0545-7>.

Hori, T., Miyazaki, S., 2010. Hierarchical asperity model for multiscale characteristic earthquakes: A numerical study for the off-Kamaishi earthquake sequence in the NE Japan subduction zone. *Geophys. Res. Lett.* 37 (10), L10304. <https://doi.org/10.1029/2010GL042669>.

Kato, A., Fukuda, J., Nakagawa, S., Obara, K., 2016. Foreshock migration preceding the 2016 Mw 7.0 Kumamoto earthquake, Japan. *Geophys. Res. Lett.* 43, 8945-8953. <https://doi.org/10.1002/2016GL070079>.

Lapusta, N., Rice, J.R., Ben-Zion, Y., Zheng, G., 2000. Elastodynamic analysis for slow tectonic loading with spontaneous rupture episodes on faults with rate- and state-dependent friction. *J. Geophys. Res.* 105 (B10), 23765-23789. <https://doi.org/10.1029/2000JB900250>.

- Lei, X., 2003. How do asperities fracture? An experimental study of unbroken asperities. *Earth Planet. Sci. Lett.* 213 (3-4), 347–359. [https://doi.org/10.1016/S0012-821X\(03\)00328-5](https://doi.org/10.1016/S0012-821X(03)00328-5).
- Moore, J.D.P., Yu, H., Tang, C.-H., Wang, T., Barbot, S., Peng, D., Masuti, S., Dauwels, J., Hsu, Y.-J., Lambert, V., Nanjundiah, P., Wei, S., Lindsey, E., Feng, L., Shibazaki, B., 2017. Imaging the distribution of transient viscosity after the 2016 *M*<sub>w</sub> 7.1 Kumamoto earthquake. *Science* 356 (6334), 163-167. <https://doi.org/10.1126/science.aal3422>.
- Nanjo, K.Z., Izutsu, J., Orihara, Y., Kamogawa, M., Nagao, T., 2019. Changes in seismicity pattern due to the 2016 Kumamoto earthquakes identify a highly stressed area on the Hinagu fault zone. *Geophys. Res. Lett.* 46, 9489-9496. <https://doi.org/10.1029/2019GL083463>.
- Nanjo, K.Z., Hirata, N., Obara, K., Kasahara, K., 2012. Decade-scale decrease in *b* value prior to the *M*<sub>9</sub>-class 2011 Tohoku and 2004 Sumatra quakes. *Geophys. Res. Lett.* 39, L20304. <https://doi.org/10.1029/2012GL052997>.
- Nanjo, K.Z., Izutsu, J., Orihara, Y., Furuse, N., Togo, S., Nitta, H., Okada, T., Tanaka, R., Kamogawa, M., Nagao, T., 2016. Seismicity prior to the 2016 Kumamoto earthquakes. *Earth Planets Space*, 68 (1), 187. <https://doi.org/10.1186/s40623-016-0558-2>.
- Nanjo, K.Z., Yoshida, A., 2017. Anomalous decrease in relatively large shocks and increase in the *p* and *b* values preceding the April 16, 2016, *M*<sub>7.3</sub> earthquake in Kumamoto, Japan. *Earth Planets Space*, 69 (1), 13. <https://doi.org/10.1186/s40623-017-0598-2>.

- Nanjo, K.Z., 2020. Were changes in stress state responsible for the 2019 Ridgecrest, California, earthquakes? *Nat. Commun.* 11, 3082. <https://doi.org/10.1038/s41467-020-16867-5>.
- Nanjo, K.Z., Yoshida, A., 2018. A *b* map implying the first eastern rupture of the Nankai Trough earthquakes. *Nat. Commun.* 9 (1), 1117. <https://doi.org/10.1038/s41467-018-03514-3>.
- Narteau, C., Byrdina, S., Shebalin, P., Schorlemmer, D., 2009. Common dependence on stress for the two fundamental laws of statistical seismology. *Nature* 462 (7273), 642-645. <https://doi.org/10.1038/nature08553>.
- National Research Institute for Earth Science and Disaster Resilience, 2016. <http://cais.gsi.go.jp/YOCHIREN/activity/211/image211/026-030.pdf> (In Japanese). Accessed April 2, 2021.
- Onaka, M., 1993. Critical size of the nucleation zone of earthquake rupture inferred from immediate foreshock activity. *J. Phys. Earth* 41 (1), 45-56. <https://doi.org/10.4294/jpe1952.41.45>.
- Omori, F., 1894. On the after-shocks of earthquakes. *Journal of the College of Science, Imperial University of Tokyo*, 7, 111-200.
- Pollitz, F.F., Kobayashi, T., Yagai, H., Shibasaki, B., Matsumoto, T., 2017. Viscoelastic lower crust and mantle relaxation following the 14-16 April 2016 Kumamoto, Japan, earthquake sequence. *Geophys. Res. Lett.* 44, 8795– 8803. <https://doi.org/10.1002/2017GL074783>.
- Scholz, C.H., 1968. The frequency-magnitude relation of microfracturing in rock and its relation to

- earthquakes. *Bull. Seismol. Soc. Amer.* 58 (1), 399-415.
- Scholz, C.H., 2015. On the stress dependence of the earthquake  $b$  value. *Geophys. Res. Lett.* 42, 1399-1402. <https://doi.org/10.1002/2014GL062863>.
- Schorlemmer, D., Neri, G., Wiemer, S., Mostaccio, A., 2003. Stability and significance tests for  $b$ -value anomalies: Example from the Tyrrhenian Sea. *Geophys. Res. Lett.* 30 (16), 1835. <https://doi.org/10.1029/2003GL017335>.
- Schorlemmer, D., Wiemer, S., 2005. Microseismicity data forecast rupture area. *Nature* 434 (7037), 1086. <https://doi.org/10.1038/4341086a>.
- Schorlemmer, D., Wiemer, S., Wyss, M., 2004. Earthquake statistics at Parkfield: 1. Stationarity of  $b$  values. *J. Geophys. Res.*, 109, B12307. <https://doi.org/10.1029/2004JB003234>.
- Schorlemmer, D., Wiemer, S., Wyss, M., 2005. Variations in earthquake-size distribution across different stress regimes. *Nature* 437 (7058), 539-542. <https://doi.org/10.1038/nature04094>.
- Shirahama, Y., Yoshimi, M., Awata, Y., Maruyama, T., Azuma, T., Miyashita, Y., Mori, H., Imanishi, K., Takeda, N., Ochi, T., Otsubo, M., Asahina, D., Miyakawa, A., 2016. Characteristics of the surface ruptures associated with the 2016 Kumamoto earthquake sequence, central Kyushu, Japan. *Earth Planets Space* 68 (1), 191. <https://doi.org/10.1186/s40623-016-0559-1>.
- Sobiesiak, M., Meyer, U., Schmidt, S., Götze, H.-J., Krawczyk, C.M., 2007. Asperity generating upper crustal sources revealed by  $b$  value and isostatic residual anomaly grids in the area of

- Antofagasta, Chile. *J. Geophys. Res.* 112, B12308. <https://doi.org/10.1029/2006JB004796>.
- Stein, R., Toda, S., 2016. How a  $M = 6$  earthquake triggered a deadly  $M = 7$  in Japan. *Temblor*.  
<https://doi.org/10.32858/temblor.009>.
- Tada, T., 1985. Spreading of the Okinawa Trough and its relation to the crustal deformation in the Kyushu (2). *Zisin* 38 (1), 1-12 (In Japanese with English abstract).  
[https://doi.org/10.4294/zisin1948.38.1\\_1](https://doi.org/10.4294/zisin1948.38.1_1).
- Tormann, T., Enescu, B., Woessner, J., Wiemer, S., 2015. Randomness of megathrust earthquakes implied by rapid stress recovery after the Japan earthquake. *Nature Geosci.* 8 (2), 152-158.  
<https://doi.org/10.1038/ngeo2343>.
- Tormann, T., Wiemer, S., Metzger, S., Michael, A., Hardebeck, J.L., 2013. Size distribution of Parkfield's microearthquakes reflects changes in surface creep rate. *Geophys. J. Int.* 193 (3), 1474-1478. <https://doi.org/10.1093/gji/ggt093>.
- Utsu, T., 1961. A statistical study on the occurrence of aftershocks. *Geophysics* 30, 521-605.
- Utsu, T., 1999. Representation and analysis of the earthquake size distribution: A historical review and some approaches. *Pure Appl. Geophys.* 155 (2-4), 509-535.  
<https://doi.org/10.1007/s000240050276>.
- Wessel, P., Smith, W.H.F., Scharroo, R., Luis, J.F., Wobbe, F., 2013. Generic Mapping Tools: Improved version released. *Eos, Transactions American Geophysical Union* 94 (45), 409-410.

<https://doi.org/10.1002/2013EO450001>.

Wiemer, S., 2001. A software package to analyze seismicity: ZMAP. *Seismol. Res. Lett.* 72 (3), 373-382. <https://doi.org/10.1785/gssrl.72.3.373>.

Woessner, J., Wiemer, S., 2005. Assessing the quality of earthquake catalogues: Estimating the magnitude of completeness and its uncertainty. *Bull. Seismol. Soc. Amer.* 95 (2), 684-698. <https://doi.org/10.1785/0120040007>.

Yagi, Y., Okuwaki, R., Enescu, B., Kasahara, A., Miyakawa, A., Otsubo, M., 2016. Rupture process of the 2016 Kumamoto earthquake in relation to the thermal structure around Aso volcano. *Earth Planets Space* 68 (1), 118. <https://doi.org/10.1186/s40623-016-0492-3>.

Yoshida, S., Kato, N., 2003. Episodic aseismic slip in a two-degree-of-freedom block-spring model. *Geophys. Res. Lett.* 30 (13), 1681. <https://doi.org/10.1029/2003GL017439>.

Zhuang, J., Ogata, Y., Wang, T., 2017. Data completeness of the Kumamoto earthquake sequence in the JMA catalog and its influence on the estimation of the ETAS parameters. *Earth Planets Space* 69, 36. <https://doi.org/10.1186/s40623-017-0614-6>.

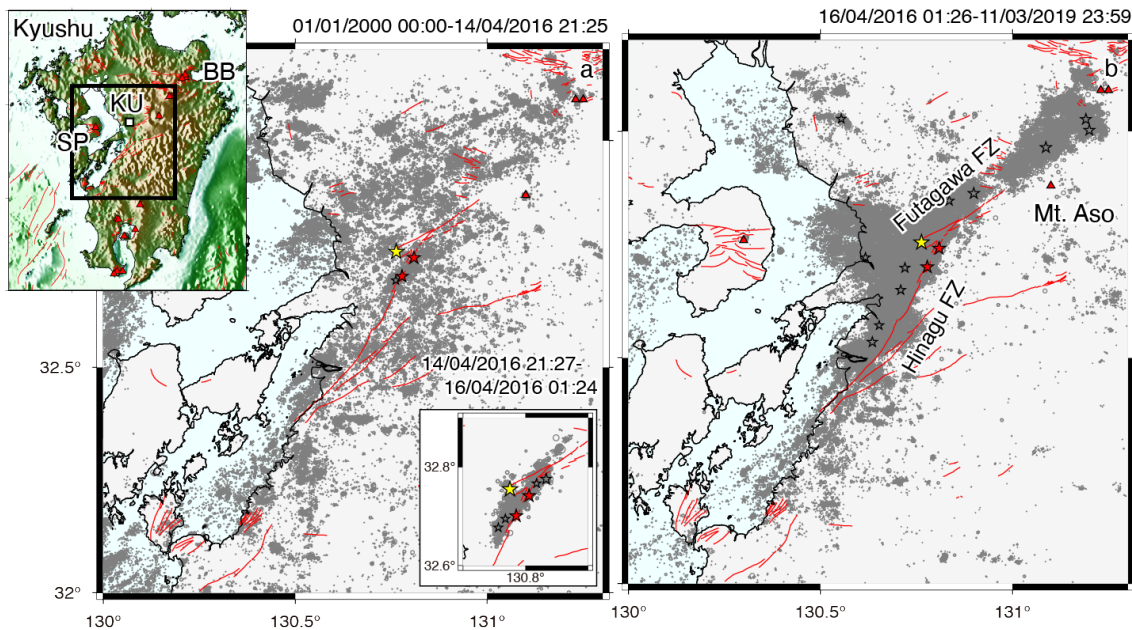


Fig. 1. The 2016 Kumamoto earthquake sequence ( $M \geq 0$ ). (a) Map of earthquakes before the start of the Kumamoto earthquakes (January 1, 2000 to April 14, 2016, 20:15). Stars show epicenters of the  $M6.5$  and  $M6.4$  foreshocks (red) and  $M7.3$  mainshock (yellow), and  $M5$  event on June 8, 2000 (open). Triangles indicate volcanoes. Red lines indicate mapped faults. Inset at the upper-left corner shows the study region (black rectangle). White square indicates the City of Kumamoto (KU). BB and SP represent Beppu Bay and Shimabara Peninsula, respectively. Inset at the lower-right corner shows a map during the period from the time of the  $M6.5$  foreshock to the time of the  $M7.3$  mainshock. Stars indicate  $M \geq 5$  events. (b) Same as (a) for aftershocks (April 16, 2016, 1:25 to March 11, 2019, 23:59).

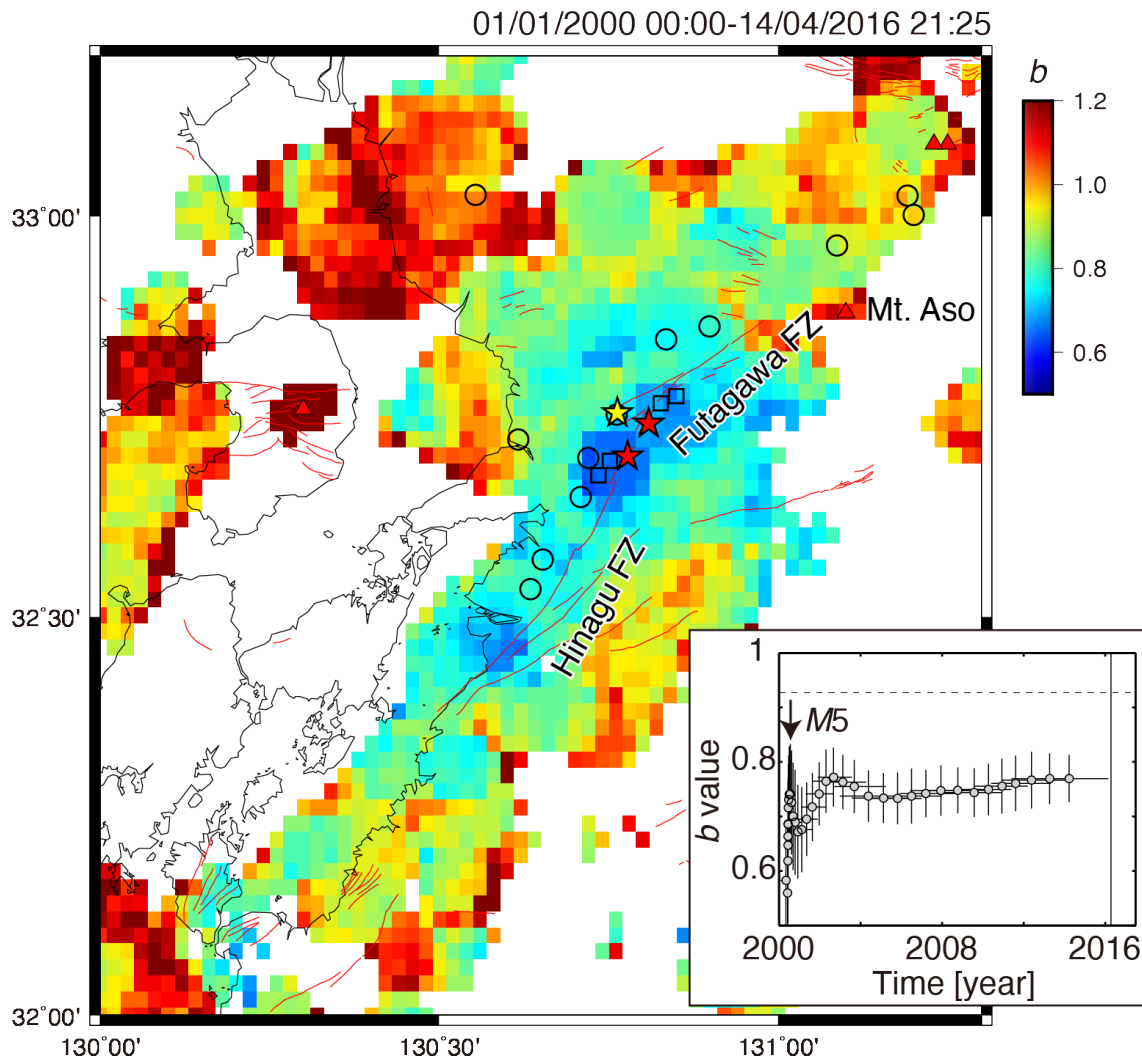


Fig. 2. Map of  $b$ -values obtained from events before the start of the Kumamoto earthquake sequence (from January 1, 2000 to immediately before the  $M6.5$  foreshock). We calculated  $b$ -values for events falling in a cylindrical volume with radius  $r = 5$  km, centered at each node on a  $0.02^\circ \times 0.02^\circ$  grid (Nanjo et al., 2016, 2019). Overlapped are the epicenters of the  $M7.3$  mainshock (yellow star),  $M6.5$ -class foreshocks (red stars),  $M \geq 5$  foreshocks (squares), and  $M \geq 5$  aftershocks (circles). Triangles indicate volcanos. Red lines indicate mapped faults. Inset shows time series of  $b$ -values based on earthquakes in the cylindrical volume with a radius  $r = 10$  km, centered at the epicenter of

the mainshock. We used a moving window approach, whereby the window covered 500 events.

$b$ -values after the fluctuation due to aftershocks of the 2000  $M5$  earthquake were stable and smaller than the regional average  $b = 0.93$ , indicated by the horizontal line (Nanjo et al., 2016). Vertical line shows moment of the start of the Kumamoto sequence.

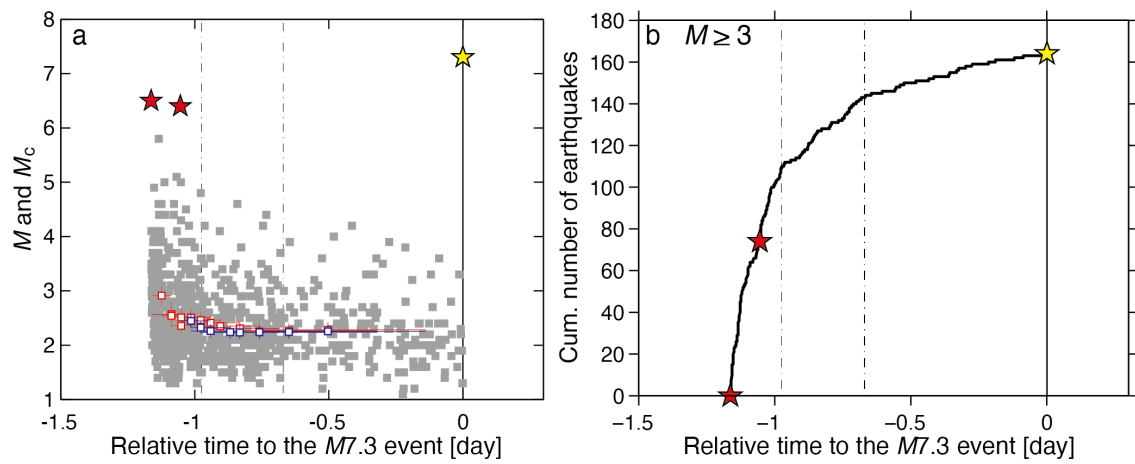


Fig. 3. Foreshock sequence (modified from Nanjo and Yoshida, 2017). (a)  $M$ -time plot. Stars show the  $M6.5$ -class foreshocks (red) and  $M7.3$  mainshock (yellow). Also included is a  $M_c$ -time plot since the  $M6.5$  foreshock (red) and the  $M6.4$  foreshock (blue). Vertical dashed lines show the relative times, 0.98 and 0.67 days, to the  $M7.3$  mainshock. Vertical solid line indicates moment of the  $M7.3$  mainshock. (b) Same as (a) for time dependence of the cumulative number of  $M \geq 3$  foreshocks.

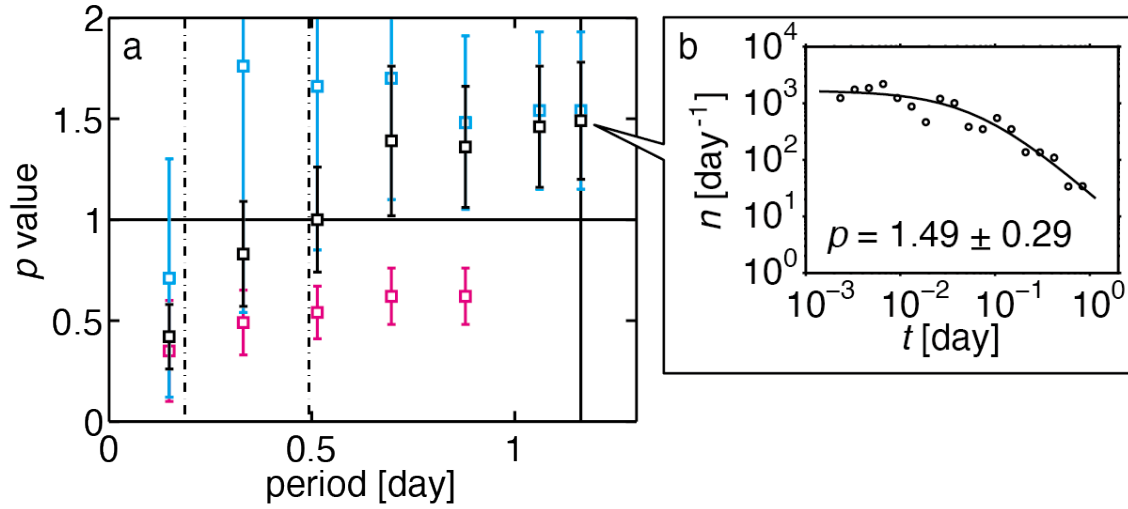


Fig. 4. The OU law fitting. (a) Plot of  $p$ -values as a function of the length of the period (days) since the  $M6.5$  foreshock for seismicity ( $M \geq 3$ ) in the entire area (black), in the northern area (blue), and in the southern area (pink). Vertical dashed lines indicate the length of the period, 0.18 and 0.49 days. Vertical solid line showing the length of the period of 1.16 days corresponds to the length of the period from the time of the  $M6.5$  foreshock to the time of the  $M7.3$  mainshock. The  $p$ -value of  $M \geq 3$  was not plotted for the southern area for periods longer than one day because the model-fitting analysis did not converge. (b) The number of  $M \geq 3$  earthquakes per day ( $n$ ) as a function of  $t$  (day) for the entire area during the period between the  $M6.5$  and  $M7.3$  earthquakes, where the  $M6.5$  foreshock was assumed to be a mainshock. The  $p$ -value ( $p = 1.49 \pm 0.29$ ) obtained for the best fitting of the OU law in Eq. (2) to data is shown by a black point on right end in Fig. 4a. The figure is modified from Nanjo and Yoshida (2017).

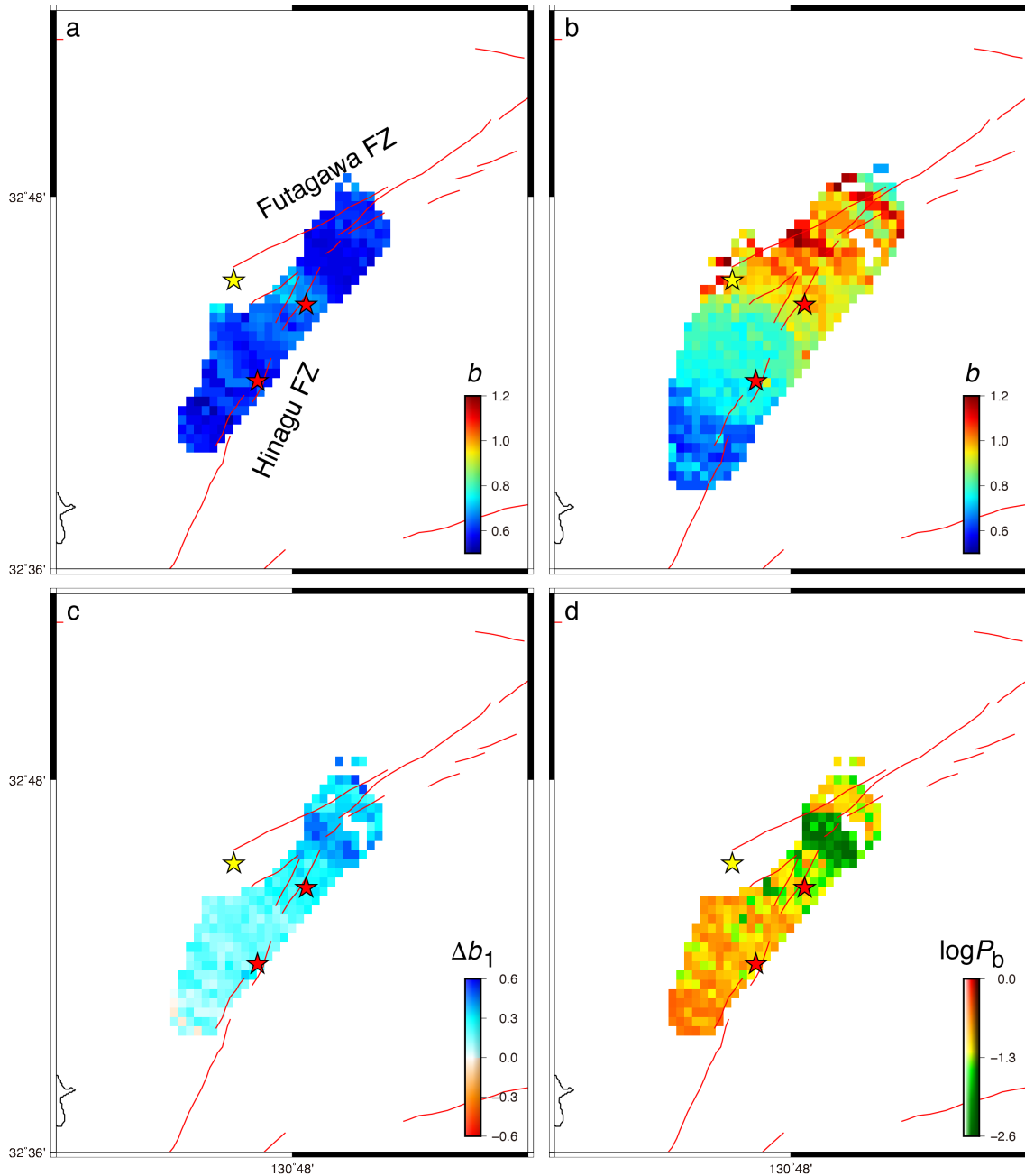


Fig. 5. Results of  $b$ -value analysis for the period from the  $M6.5$  foreshock to the  $M7.3$  mainshock (modified from Nanjo and Yoshida, 2017). (a) Maps of  $b$ -values for seismicity during the period 1.16-0.98 days prior to the  $M7.3$  mainshock. The mapping procedure is the same as that for Fig. 2, except for a smaller node spacing ( $0.005^\circ \times 0.005^\circ$ ). (b) Same as (a) for the period 0.98-0 days. (c,d)

$\Delta b_1$  and  $\log P_b$  for the periods 1.16-0.98 and 0.98-0 days, where  $\Delta b_1 = b_{1.16-0.98} - b_{0.98-0}$ .

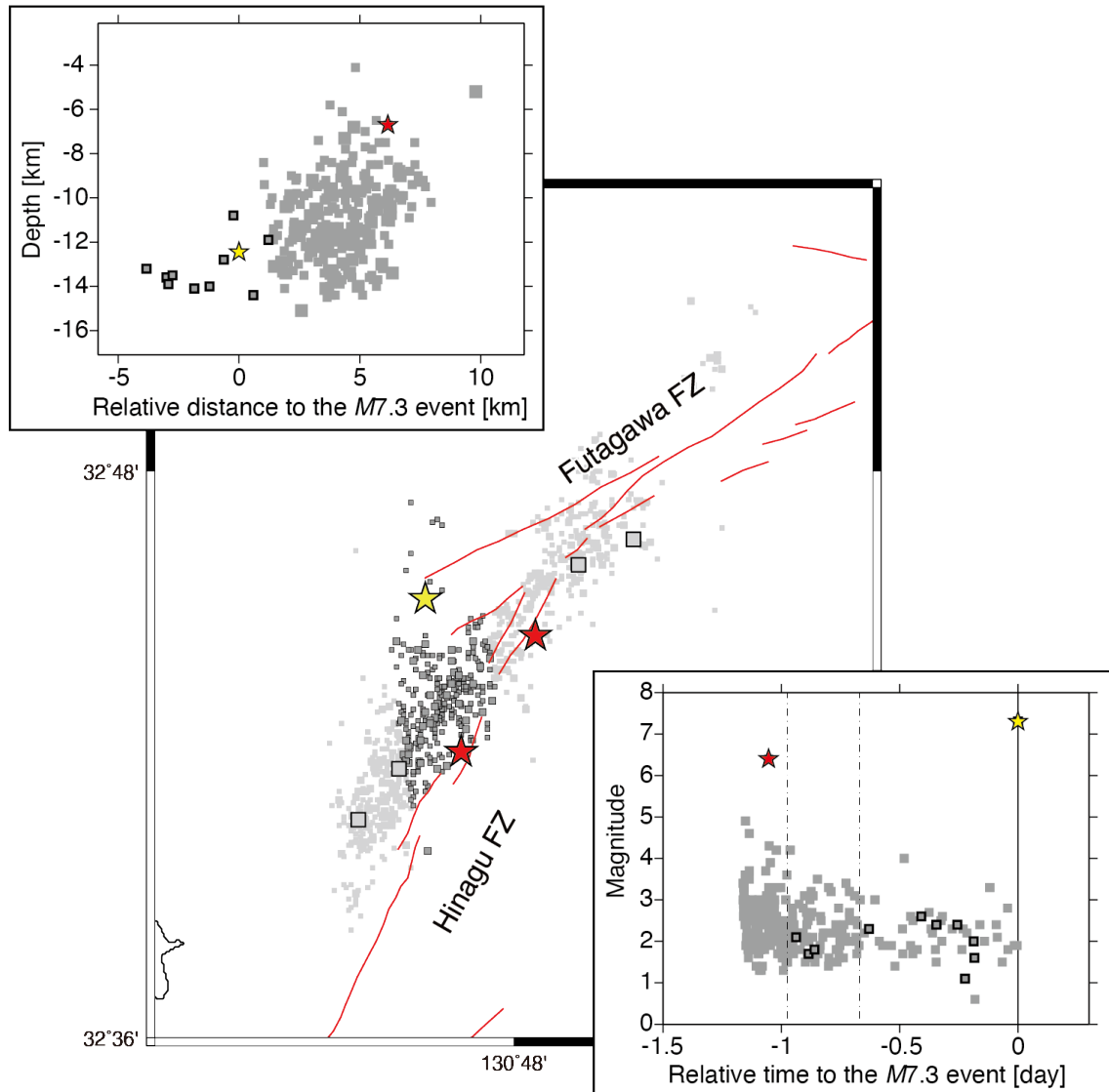


Fig. 6. Same as the inset of Fig. 1a, but events used to create a 5-km-wide cross-sectional view of the upper-left-corner inset and  $M$ -time diagram of the lower-right-corner inset are highlighted by dark grey. The  $M7.3$  mainshock,  $M6.5$ -class foreshocks, and  $M \geq 5$  foreshocks are shown by a yellow star, red stars, and large squares, respectively. Upper-left-corner inset: Apart from the majority of events, outliers (bold squares) are observed around the hypocenter of the  $M7.3$  mainshock.

Lower-right-corner inset: Outliers seen in the cross-sectional view of the upper-left-corner inset are indicated by bold squares. Vertical dashed lines show the relative times, 0.98 and 0.67 days, to the  $M7.3$  mainshock. Vertical solid line indicates the moment of the  $M7.3$  mainshock. The figure is modified from Nanjo and Yoshida (2017).

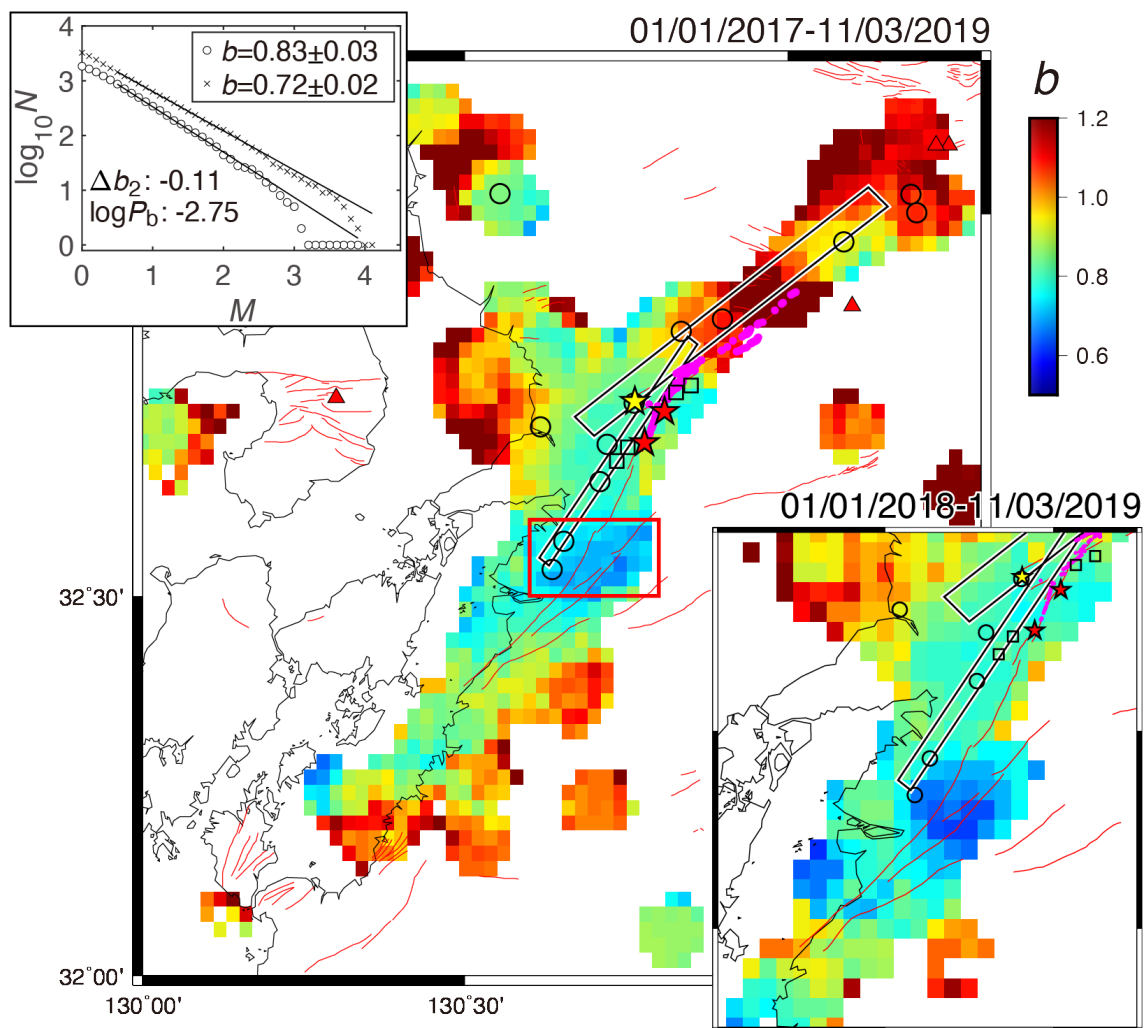


Fig. 7. Same as Fig. 2 for the period after the  $M7.3$  mainshock (from January 1, 2017 to March 11, 2019). Superimposed are after-slip planes (black rectangles) used by Pollitz et al. (2017). We checked if the extent of the observed surface rupture (magenta; Shirahama et al., 2016) corresponds

to that of the area with a significant change in  $b$ -value and found no clear correlation. Inset at the upper-left corner shows the GR fitting in Eq. (1) to seismicity in the red rectangular region shown in the main figure before and after the Kumamoto earthquakes, where circles and crosses indicate seismicity used for Fig. 2 ( $M_c = 0.5$ ,  $b_{\text{pre}} = 0.83 \pm 0.03$ , and  $a = 3.35$ ) and for the main figure ( $M_c = 0.5$ ,  $b_{\text{post}} = 0.72 \pm 0.02$ , and  $a = 3.52$ ), respectively. The difference in  $b$  ( $\Delta b_2 = b_{\text{post}} - b_{\text{pre}}$ ), indicated by  $\log P_b = 2.75$ , is significant. This significance is further supported by noting that the absolute difference in  $b$  is larger than the sum of uncertainties of the  $b$ -values. The significant change in  $b$  holds true ( $\Delta b_2 = -0.12$ ,  $\log P_b = -2.09$ ) when comparing with the  $b$ -value based on seismicity since January 1, 2018 with ( $M_c = 0.5$ ,  $b_{\text{post}} = 0.71 \pm 0.03$ ,  $a = 3.04$ ). Inset at the lower-right corner indicates a zoomed-in  $b$ -value map for seismicity during the period from January 1, 2018 to March 11, 2019. The figure is modified from Nanjo et al. (2019).

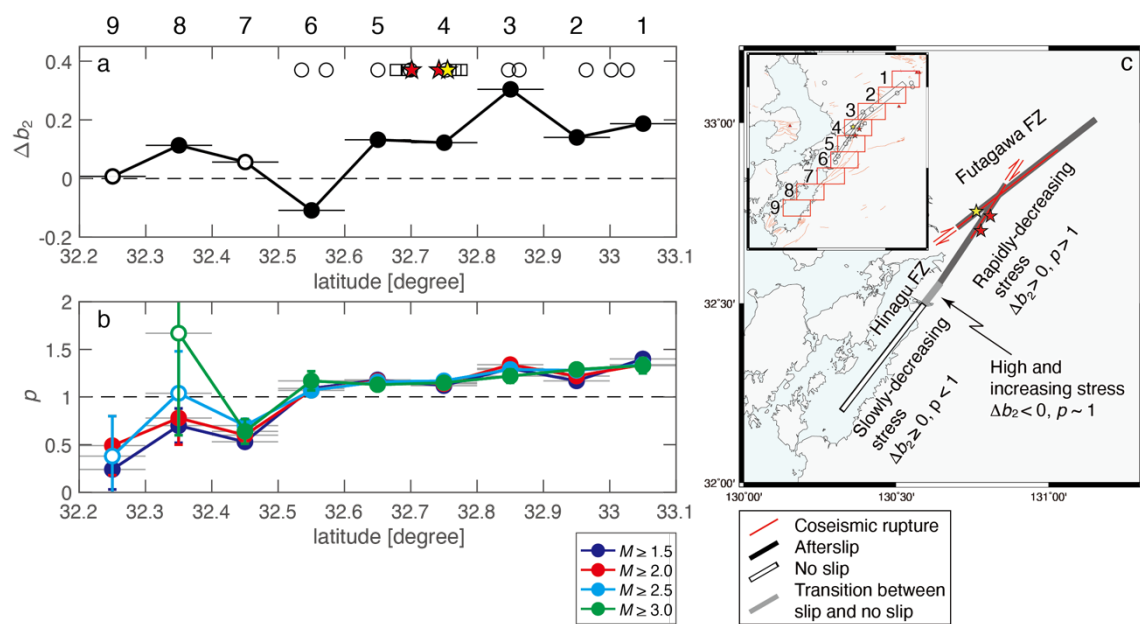


Fig. 8. Results of  $b$ - and  $p$ -values along the Futagawa-Hinagu FZ (modified from Nanjo et al., 2019).

(a)  $\Delta b_2$  ( $= b_{\text{post}} - b_{\text{pre}}$ ) as a function of latitude, where  $b_{\text{pre}}$  and  $b_{\text{post}}$  were computed based on seismicity used to create Fig. 2 and the main figure of Fig. 7, respectively, and data with  $\log P_b > -1.3$  are shown by open circles. The numbers (1, 2, ..., 9) appearing on the margin of the figure (a) correspond to the region numbers shown in the inset of (c). Yellow and red stars show latitudes of the  $M7.3$  mainshock and  $M6.5$ -class foreshocks, respectively. Circles and squares indicate  $M \geq 5$  aftershocks and foreshocks, respectively. (b)  $p$ -value for seismicity after the  $M7.3$  mainshock for different lower cut-off magnitudes as a function of latitude. Open circles show  $p$ -values obtained based on  $N \leq 20$  earthquakes. The  $p$ -value of  $M \geq 3$  was not plotted for Region 9, because the model-fitting analysis did not converge. (c) Summary map showing all of the observations and visualizing the stress model. Red lines indicate the coseismic ruptures of the  $M7.3$  mainshock and  $M6.5$ -class foreshocks with the sense of fault slip represented by pairs of red half-arrows (ERC, 2016a; Yagi et al., 2016). Black lines represent after-slip planes showing the Futagawa FZ and the northern section of the Hinagu FZ (Pollitz et al., 2017) in the after-slip-dominant regime. Outlined line indicates the southern section of the Hinagu FZ in the viscoelastic-flow-dominant regime, where no slips (no coseismic ruptures and no after-slips) occurred. Gray segment indicates the boundary between the zones with and without slips, where  $b$ -values show a decrease over time (increasing stress), to low values (indicative of high stress). Inset shows Regions 1-9 (rectangles) considered for

(a,b). Region 6 corresponds to the region shown in Fig. 7.